Postprint of: Abdullah M., Kozieł S., Supervised-learning-based development of multi-bit RCS-reduced coding metasurfaces, IEEE TRANSACTIONS ON MICROWAVE THEORY AND TECHNIQUES Vol. 70 No 1 (2021), pp. 264-274, DOI: 10.1109/TMTT.2021.3105677

Supervised-Learning-Based Development of Multibit RCS-Reduced Coding Metasurfaces

Muhammad Abdullah and Slawomir Koziel, *Senior Member, IEEE*

***Abstract*— Coding metasurfaces have been introduced as efficient tools allowing meticulous control over the electromagnetic (EM) scattering. One of their relevant application areas is radar cross section (RCS) reduction, which principally relies on the diffusion of impinging EM waves. Despite its significance, careful control of the scattering properties poses a serious challenge at the level of practical realization. This article is concerned with (global) design optimization of coding metasurfaces featuring broadband RCS reduction. We adopt a two-stage optimization procedure involving data-driven supervised-learning, sequential-search strategy, and direct EM-based design closure of the entire metasurface oriented toward maximizing the RCS reduction bandwidth. Our framework is then used to develop a two-bit coding metasurface. To handle the combinatorial explosion at the concurrent meta-atom optimization stage, a sequential-search strategy has been developed that enables global search capability at low computational cost. Finally, EM-based optimization is executed to maximize RCS reduction bandwidth at the level of entire metasurface. The properties of the coding metasurface are demonstrated using monostatic and bistatic RCS performance. The 10-dB RCS reduction can be obtained in the frequency range of 14.8–37.2 GHz, in a monostatic configuration. Also, 15-dB RCS reduction can be maintained in the frequency range of 16.7–37 GHz. Simulations are validated using physical measurements of the fabricated prototypes. Finally, the performance of the structure is benchmarked against recently reported designs.**

***Index Terms*— Beam manipulation, coding metasurface, diffusion, multibit coding, radar cross section (RCS), supervised learning.**

I. Introduction

With the advancements in radar detection methods, improving stealthiness of aircrafts has become a forefront of research within the stealth technology [1]–[3]. Conventional approaches adopted to accomplish the stealth features commonly involve shape and material stealth [4]. The former impacts the aerodynamic performance and structural integrity of the aircraft. The latter suffers from the increased thickness, weight, and cost. A relatively new class of artificially engineered materials, or metamaterials, has recently become a viable alternative to conventional stealth approaches.

A metasurface is a planar patterned surface composed of subwavelength periodic arrays of meta-atoms (or unit cells), offering extraordinary characteristics [5]. Until now, metasurfaces are developed as either absorbing metasurfaces [6]–[8] or scattering manipulation metasurfaces [9]–[23]. The former ones are designed to convert the electromagnetic (EM) wave energy into heat and dissipate it. These metasurfaces are susceptible to infrared detectors, which increases their detection probability. In 2011, Yu *et al.* [9] proposed a generalized Snell's law, followed by the introduction of the idea of scattering manipulation [10] and, finally, the design of the metasurface composed of V-shaped meta-atoms [10]. Therein, the phase and the amplitude of the EM wave can be effectively manipulated by changing the meta-atom geometry. Also, the weight, thickness, and losses of the structure can be maintained below a certain, practically acceptable level. These attributes make the scattering control metasurfaces a hotspot in the stealth research.

Contemporary metasurfaces can be classified into single-beam [9], [10], multibeam [11]–[13], and the diffusion metasurfaces [14]–[19]. The single-beam scattering metasurfaces offer radar cross section (RCS) reduction in a monostatic configuration; however, they are not effective to reduce bistatic RCS, essential in the context of multibase radar detection technology. To realize RCS reduction in a bistatic regime, it is important to increase the number of scattering beams. One example is a checkerboard metasurface [13], employing two distinct meta-atom designs in a chessboard configuration. The two meta-atoms represents two-phase states (0 and π) to realize essential RCS reduction [13]. However, a limited number of scattering beams and a fixed beam propagation direction limit the widespread utility of a checkerboard metasurface. To further increase the number of scattering beams, the idea of diffusion metasurface (also referred to as a coding metasurface) has been presented [14]–[16], featuring a random arrangement of the meta-atoms. This leads to the increased number of scattered beams and, hence, successful bistatic RCS reduction. In [15] and [16], the coding diffusion metasurfaces are exploited to achieve the required RCS reduction performance. Yet, the RCS reduction performance of such structures is limited up to 50° angle of incidence (as in [15]). In this class of metasurfaces, the major scattering directions remain within

Manuscript received July 4, 2021; accepted August 3, 2021. This work was supported in part by the Icelandic Centre for Research (RANNIS) under Grant 206606051 and in part by the National Science Centre of Poland under Grant 2017/27/B/ST7/00563. *(Corresponding author: Muhammad Abdullah.)*

Muhammad Abdullah is with the Engineering Optimization and Modeling Center, Reykjavik University, 102 Reykjavik, Iceland (e-mail: muhammada19@ru.is).

Slawomir Koziel is with the Engineering Optimization and Modeling Center, Reykjavik University, 102 Reykjavik, Iceland, and also with the Faculty of Electronics, Telecommunications and Informatics, Gdańsk University of Technology, 80-233 Gdańsk, Poland (e-mail: koziel@ru.is).

Color versions of one or more figures in this article are available at https://doi.org/10.1109/TMTT.2021.3105677.

Digital Object Identifier 10.1109/TMTT.2021.3105677

a certain angular range, which might have adverse effects on the RCS performance. The absence of rigorous methods of predicting and controlling the allocation of the scattered beams hinders the widespread use of diffusion metasurfaces. Their backscattering characteristics solely rely on the geometrical structure of meta-atoms. To provide additional degrees of freedom and to facilitate the manipulation of EM waves, four types of meta-atom designs representing four phase states (0, $\pi/2$, π, and $3\pi/2$) can be utilized as a building block of a two-bit coding metasurface [20], [21]. However, the development of such architectures involves concurrent optimization of the meta-atoms. The lack of efficient techniques to optimize individual meta-atoms and the entire metasurface limits the performance of multibit coding metasurfaces, in particular, their RCS reduction bandwidth.

Conventional metasurface design methodologies employ empirical reasoning and intuition-inspired practices. The two design stages involved in the process are the design and optimization of individual meta-atoms, followed by the optimization of the entire metasurface. Due to the absence of reliable analytical models, the only practical choice is experience-driven design methods. Unfortunately, such approaches exhibit limited efficacy as well as capability to identify truly optimum designs. Efficient development of multibit metasurfaces requires innovative algorithmic solutions, capable of tacking the aforementioned downsides. The developments in high-performance computing have dramatically boosted the utility of rigorous EM-driven design procedures, principally based on numerical optimization [24]. However, direct EM-based optimization of complex structures using conventional algorithms may be prohibitively expensive, especially if global exploration is needed. A practical solution might be the utilization of supervised machine learning [25], involving metamodeling [26]–[29]. Shifting the computational overhead to a cheaper metamodel, implementing a sequential-search strategy, and finally incorporating other means such as problem decomposition [31] may enable efficient development of complex multibit metasurfaces, otherwise impractical.

This work proposes a novel algorithmic framework for global optimization of two-bit coding metasurface featuring broadband RCS reduction performance. The metasurface is composed of lattices featuring four unique geometries of meta-atoms to mimic "00," "01," "10," and "11" binary codes, standing for a phase reflection state of 0, $\pi/2$, π, and $3\pi/2$, respectively. The optimization procedure adopted in this work involves a data-driven supervised-learning technique [32], sequential-search strategy to face combinatorial explosion and permit global exploration, as well as EM-based local optimization of the entire structure at hand. It should be noted that the concept of supervised-learning-based optimization procedure has been adopted from [32]; however, the global optimization procedure (the sequential-search algorithm) has been developed specifically to tackle the challenges pertinent to handling four meta-atoms, where the original approach of [32] would not work due to excessive computational costs. Supervised learning involves sampled EM simulation data, with the surrogate model implemented using kriging interpolation [25]. The latter serves as a meta-atom phase characteristic predictor during the global optimization stage. The sequential-search strategy is introduced to decompose the optimization task by gradually increasing the pool of simultaneously considered pairs of meta-atoms, thus effectively administering the computational overhead. This turns instrumental in handling the task, otherwise computationally prohibitive considering the large dimensionality of the parameter space. At the EM-based local optimization stage, a trust-region (TR) gradient algorithm with sparse sensitivity updates [31] and a regularization approach is applied to expedite the optimization procedure and to efficiently handle frequency-localized violations of assumed level of the RCS reduction.

The adopted algorithmic solution addresses the key challenges pertinent to global optimization of meta-atom designs in a fully automated manner. It has been applied to develop a multibit coding metasurface featuring 10-dB RCS reduction in a frequency range from 14.8 to 37.5 GHz. The design is validated both numerically and experimentally and shown to outperform the state-of-the-art benchmark structures with respect to the RCS reduction bandwidth and the level RCS reduction.

The technical novelty and major contributions of this article can be summarized as follows: 1) development of an algorithmic solution to enable systematic and globally optimum meta-atom designs; 2) development of sequential approach for global optimization of meta-atoms to address the issue of combinatorial explosion when handling simultaneous parameter tuning of multiple unit cells; 3) development of alternative objective function formulation for efficient EM-driven design closure of the metasurface, addressing the problem of discontinuities due to localized violations of the acceptance threshold for the RCS reduction; 4) corroborating the efficacy of the design procedure as well as demonstrating its practical utility in the context of complex metasurface design and optimization; and 5) the employment of the proposed algorithmic framework to the development of a high-performance two-bit coding metasurface for broadband RCS reduction. It should be emphasized that the proposed algorithmic solution is—to the authors' best knowledge—the first endeavor in the literature to ensure globally optimum meta-atom designs, indispensable in the development of complex multibit coding metasurfaces. At the same time, it should be reiterated that the primary point of interest and the scope of the article are numerical optimization of multibit coding metasurfaces, in particular introduction of a procedure for identifying globally optimum parameter setup and providing the means that allow us to solve numerical challenges that arise on the way (cf. points (ii) and (iii) mentioned above). Proposing methods for RCS reduction is outside the scope of this work. The considered specific metasurface design is discussed merely as a demonstration example for the algorithmic framework.

This article is organized as follows. In Section II, we introduce the geometry and EM modeling of the exemplary meta-atom, subsequently used to develop the RCS reduction metasurface and to demonstrate the considered algorithmic solution. Section III provides the comprehensive description of the supervised-learning-enabled concurrent meta-atom optimization procedure. Section IV discusses the

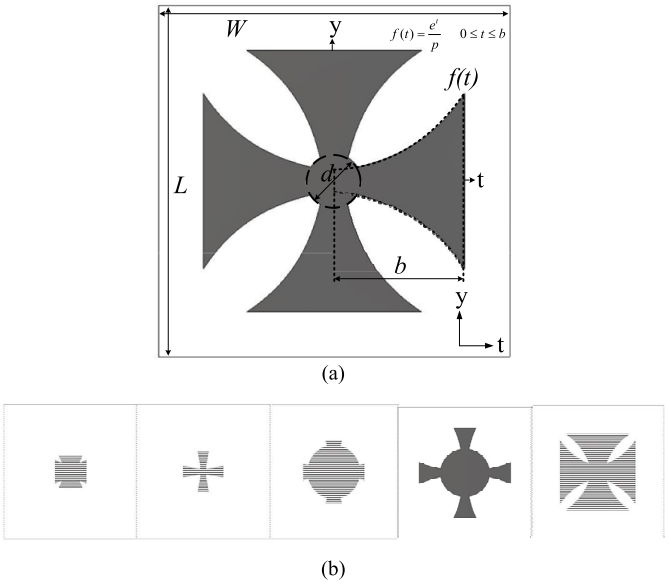

(a)

(b)

Fig. 1. Configuration of the meta-atom considered in this work. (a) Crusader cross topology. (b) Five exemplary meta-atom geometries within the parameter space.

optimization results, followed by a demonstration of a two-bit coding metasurface and its experimental validation. Section V concludes this article.

II. Geometry Configuration of Meta-Atoms and Coding Metasurface

This section describes the topology of a considered meta-atom (metasurface building block). It also contains a brief discussion concerning the coding sequence applied in the development procedure of a two-bit coding metasurface utilized to demonstrate the algorithmic framework proposed in the work.

A. Meta-Atom Geometry

Fig. 1(a) shows the geometry of a meta-atom design considered in this work. The underlying topology is borrowed from [32], and it resembles the crusader cross. The geometry is parameterized as

$$f(t) = \frac{e^t}{p}, \quad 0 \le t \le b \tag{1}$$

where p, b, and d, are the designable variables that determine the overall structure of the meta-atom. The considered geometry offers ample flexibility in the meta-atom design [cf. Fig. 1(b)] while using a small number of designable variables. The latter facilitates the supervised-learning-based modeling process and, in particular, ensures the reliability of the replacement model without incurring excessive computational expenses. Fig. 1(b) shows the geometrical flexibility of the considered meta-atom design, i.e., broad ranges of visually distinct topologies that can be generated using the basic geometry of Fig. 1(a).

A ground-backed Arlon AD250 is modeled as a dielectric layer with a relative permittivity of ($\varepsilon_r = 2.5$), a loss tangent of ($\tan\delta = 0.0018$), and a thickness of ($h = 1.5$ mm). Perfect electrical conductor (PEC) is selected as the metallic material in the computational (EM simulation) model. The overall size of the meta-atom is $W \times L = 6 \times 6$ mm^2.

11	11	11	11
10	10	10	10
01	01	01	01
00	00	00	00

Fig. 2. Coding sequence applied to develop 4 × 4 diffusion metasurface.

B. Coding Sequence of a Two-Bit Coding Metasurface

The development of a two-bit coding metasurface requires the utilization of four meta-atom designs. Consequently, the coding sequence encompassing four atoms is sophisticated than that corresponding to the standard chessboard configuration involving only two atoms. Here, the four atoms are represented as "00," "01," "10," and "11," in the arrangement shown in Fig. 2. Each atom represents a phase reflection state of 0, $\pi/2$, π, and $3\pi/2$, respectively. As presented, the entire matrix includes sixteen lattices, arranged in a 4 × 4 configuration.

III. Supervised-Learning-Enabled Metasurface Optimization Framework

This section briefly describes the implementation of a supervised-learning-based design procedure. We start by summarizing the complete procedure, followed by a discussion of the major components of the two-stage optimization procedure.

A. Design Approach Summary

The complete metasurface design procedure consists of two independent optimization stages. The first stage involves construction of a fast replacement model (surrogate) of the meta-atom within the parameter space determined by the lower and upper bounds of designable variables. Here, the allocation of the training samples on a rectangular grid is followed by data acquisition through EM simulations of the meta-atom computational model. The surrogate itself is rendered using kriging interpolation. The trained model is utilized as a prediction tool for global exploration of the parameter space. The latter is computationally prohibitive when executed directly at the level of the EM simulation model. Low dimensionality of the parameter space allows sufficient prediction power of the surrogate and thus to eliminate EM analysis from the global exploration stage altogether. Furthermore, the global search is carried out in a sequential manner to efficiently handle combinatorial explosion pertinent to concurrent optimization of four meta-atoms. Finally, EM-driven optimization of the entire metasurface is performed to directly extend the RCS

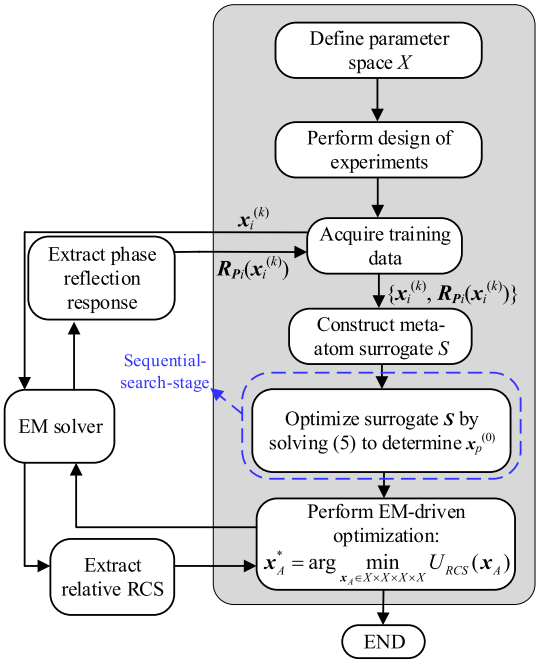

Fig. 3. Flow diagram of the supervised-learning-based design procedure.

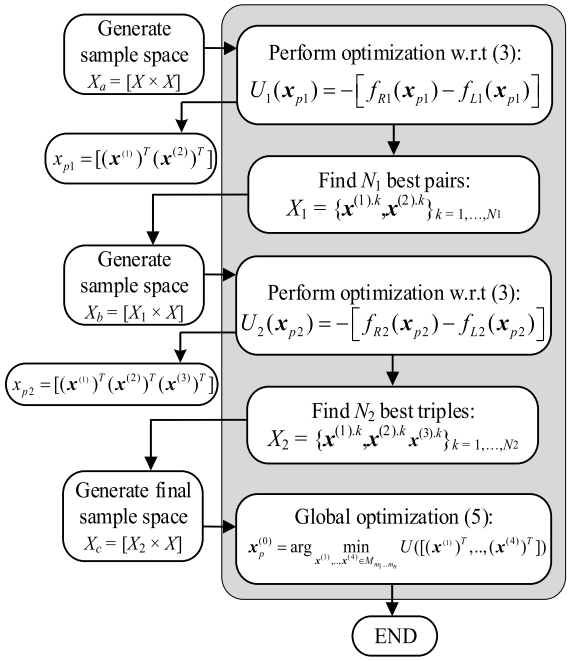

Fig. 4. Algorithmic flow of a sequential-search stage (cf. Fig. 3).

reduction bandwidth. The flow diagram of the complete design optimization procedure along with a separate illustration of the global search stage is shown in Figs. 3 and 4, respectively. The details concerning individual parts of the process are provided in the remaining part of this section.

B. Data-Driven Modeling and Concurrent Optimization of Meta-Atoms

The initial optimization stage involves data-driven meta-models [32]. It determines four globally optimum meta-atom designs exhibiting the phase difference within the range of $\{j\pi/2 \pm \alpha_{\max}\}_{j=1,2,3}$ over a possibly broad frequency range F. The threshold $\alpha_{\max}$ is set to 37°, considering practical recommendations in the literature (see [13]). These phases are understood as pertaining to the first and the second meta-atom ($\pi/2 \pm\alpha_{\max}$), the second and the third meta-atom ($2\pi/2 \pm\alpha_{\max}$), and the third and the fourth atom ($3\pi/2 \pm\alpha_{\max}$).

The vector of designable variables and the response of the EM simulation model will be denoted as $\boldsymbol{x} = [x_1, \ldots, x_n]^T \in X$ and $\boldsymbol{R}_P(\boldsymbol{x})$, respectively. The latter represents the phase reflection characteristics of the corresponding meta-atom design.

The parameter space X is defined by the lower and upper bounds $\boldsymbol{l} = [l_1, \ldots, l_n]^T$ and $\boldsymbol{u} = [u_1, \ldots, u_n]^T$ such that $l_l \le x_l \le u_l$, $l = 1, \ldots, n$.

The data acquisition is accomplished by uniformly allocating N samples within the parameter space X and obtaining their corresponding EM simulation responses. Therein, the surrogate model $\boldsymbol{S}$ is trained by means of kriging interpolation [25]. The model is identified using the training samples $\{\boldsymbol{x}^{(k)}, \boldsymbol{R}_P(\boldsymbol{x}^{(k)})\}_{k=1,\ldots,N}$. The samples are allocated on a rectangular grid, with the number of grid nodes along each parameter space axis decided based on a large-scale sensitivity analysis. This design of experiments is suitable for low-dimensional parameter spaces. The kriging model uses the first-order polynomial as a trend function and a Gaussian correlation function.

The surrogate model is employed to carry out global optimization of the four meta-atom designs, aiming at identification of the variable vectors $\boldsymbol{x}^{(j)*}$, $j = 1$, 2, 3, and 4, such that that the phase differences at the level of the surrogate model, i.e., $\Delta P(\boldsymbol{x}^{(j)*}, \boldsymbol{x}^{(j+1)*}) = \boldsymbol{S}(\boldsymbol{x}^{(j)*}) - \boldsymbol{S}(\boldsymbol{x}^{(j+1)*})$, simultaneously conform to

$$\frac{j\pi}{2} - \alpha_{\max} \le \Delta P\left(\boldsymbol{x}^{(j)*}, \boldsymbol{x}^{(j+1)*}\right) \le \frac{j\pi}{2} + \alpha_{\max} \tag{2}$$

for $j = 1$, 2, and 3, over a possibly wide range of frequencies. As mentioned before, we set $\alpha_{\max} = 37°$. Using the aggregated variable vector where the objective function U is defined as

$$\boldsymbol{x}_p = \left[(\boldsymbol{x}^{(1)})^T\ (\boldsymbol{x}^{(2)})^T\ (\boldsymbol{x}^{(3)})^T\ (\boldsymbol{x}^{(4)})^T\right]^T \tag{3}$$

the design task can be formulated as follows:

$$\boldsymbol{x}_p^* = \arg\min_{\boldsymbol{x}_p \in X\times X\times X\times X} U(\boldsymbol{x}_p). \tag{4}$$

The objective function U is defined as

$$U(\boldsymbol{x}_p) = -\left[f_R(\boldsymbol{x}_p) - f_L(\boldsymbol{x}_p)\right] \tag{5}$$

where f_L and f_R are the frequencies determining the largest continuous frequency range for which the phase difference condition (2) is satisfied for all frequencies $f \in [f_L, f_R]$.

Having a fast surrogate model, the intention is to perform a global grid-constrained exhaustive search, followed by a local refinement. We denote by $M_{m1,\ldots,mn}$ a rectangular grid defined so that $\boldsymbol{x} \in M_{m1,\ldots,mn}$ if and only if $\boldsymbol{x} = [x_1, \ldots, x_n]^T$ is of the form $x_k = l_k + j_k[(u_k - l_k)/m_k]$, $k = 1, \ldots, n$, where m_k is a grid-defining integer for the kth variable and $j_k \in \{0, 1, \ldots, m_k\}$. Exhaustive search entails solving the problem

$$\boldsymbol{x}_p^{(0)} = \arg\min_{\boldsymbol{x}^{(1)},\ldots,\boldsymbol{x}^{(4)} \in M_{m_1,\ldots,m_n}} U([(\boldsymbol{x}^{(1)})^T, \ldots, (\boldsymbol{x}^{(4)})^T]). \tag{6}$$

Unfortunately, with four meta-atoms, we face combinatorial explosion: assuming, for the sake of example, that the grid $M_{m1,\ldots,mn}$ has $N_0 = 1000$ nodes, the number of designs to consider is 10^{12}, which is computationally prohibitive even with a fast surrogate. Here, in order to address this issue, a sequential procedure is implemented as follows.

1) Consider the first two meta-atoms. Among all combinations $\boldsymbol{x}^{(1)}$, $\boldsymbol{x}^{(2)} \in M_{m1,\ldots,mn}$, and select N_1 best pairs $X_1 = \{\boldsymbol{x}^{(1).k}, \boldsymbol{x}^{(2).k}\}_{k=1,\ldots,N1}$, with respect to the objective function $U_1(\boldsymbol{x}_{p1}) = U_1([(\boldsymbol{x}^{(1)})^T(\boldsymbol{x}^{(2)})^T])$, where $U_1(\boldsymbol{x}_{p1}) = -\big[f_{R1}(\boldsymbol{x}_{p1}) - f_{L1}(\boldsymbol{x}_{p1})\big]$, with f_{L1} and f_{R1} being the frequencies determining the largest continuous frequency range for which the condition (2) is satisfied within $f \in [f_{L1}, f_{R1}]$ for $j = 1$.
2) Consider the first three meta-atoms. Among all combinations $\boldsymbol{x}^{(1)}$, $\boldsymbol{x}^{(2)}$, and $\boldsymbol{x}^{(3)}$ such that $\{\boldsymbol{x}^{(1)}, \boldsymbol{x}^{(2)}\} \in X_1$ and $\boldsymbol{x}^{(3)} \in M_{m1,\ldots,mn}$, select N_2 best triples $X_2 = \{\boldsymbol{x}^{(1).k}, \boldsymbol{x}^{(2).k}, \boldsymbol{x}^{(3).k}\}_{k=1,\ldots,N1}$, with respect to the objective function $U_2(\boldsymbol{x}_{p2}) = U_1([(\boldsymbol{x}^{(1)})^T(\boldsymbol{x}^{(2)})^T(\boldsymbol{x}^{(3)})^T])$, where $U_2(\boldsymbol{x}_{p2}) = -[f_{R2}(\boldsymbol{x}_{p2}) - f_{L2}(\boldsymbol{x}_{p2})]$, with f_{L2} and f_{R2} being the frequencies determining the largest continuous frequency range for which the condition (2) is satisfied within $f \in [f_{L2}, f_{R2}]$ for $j = 1$ and 2 simultaneously.
3) Consider all four meta-atoms. Among all combinations $\boldsymbol{x}^{(1)}$, $\boldsymbol{x}^{(2)}$, $\boldsymbol{x}^{(3)}$, and $\boldsymbol{x}^{(4)}$ such that $\{\boldsymbol{x}^{(1)}, \boldsymbol{x}^{(2)}, \boldsymbol{x}^{(3)}\} \in X_2$ and $\boldsymbol{x}^{(4)} \in M_{m1,\ldots,mn}$, find the best vector $\boldsymbol{x}_p^{(0)}$ according to the objective function (6).

Note that the number of combinations that have to be considered at steps 2 and 3 of the above procedure is only N_0N_1, instead of N_0^3 and N_0^4, respectively. Thus, the overall number of considered grid node combinations is only $N_0(N_0 + 2N_1)$, which would be $3N_0^3$ if $N_1 = N_0$ is selected (as in our actual numerical experiments). Again, assuming $N_0 = 1000$ (in practice, less than that, cf. Section IV-A), the reduction of cost is six orders of magnitude. At the same time, the probability of finding a truly optimum design this way is very high because it is extremely likely that the global optimum of (6) will be among the best N_1 combinations of the first two meta-atoms contained in X_1 and even more so among the best N_1 combinations of the first three meta-atoms contained in X_2.

The design $\boldsymbol{x}_p^{(0)}$ is further refined using standard gradient-based search at the level of the surrogate $\boldsymbol{S}$. This is to improve the resolution beyond the initial grid $M_{m1,\ldots,mn}$. When using the above-described surrogate-assisted sequential procedure, the computational cost of the global optimization stage is low.

C. EM-Driven Design Optimization of Entire Metasurface

Following global optimization of the meta-atoms, EM-driven refinement of the entire metasurface is needed. The latter is indispensable as the optimized meta-atoms do not directly translate into optimum design of the entire structure; recall that meta-atoms were tuned to satisfy the phase difference condition (2), whereas the ultimate goal is to maximize the RCS reduction bandwidth, and therefore, the enhancement has to be performed directly. Moreover, due to high computational cost incurred by structure evaluation, TR gradient-based algorithm is the only practical choice. Even in that case, certain acceleration mechanisms should be incorporated to reduce the CPU overhead to acceptable levels.

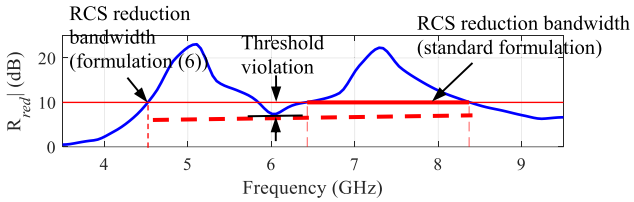

Fig. 5. Exemplary RCS reduction characteristics representing potential practical issues. The thick red horizontal line represents the RCS bandwidth (B_{RCS}) according to the standard formulation, whereas the dashed red horizontal line represents B_{RCS} as defined by (7). If the RCS reduction characteristics changes in the course of the optimization process to create the acceptance threshold violation as shown in the picture, a large discontinuity of the bandwidth will be observed (when evaluated using the standard formulation), which is problematic to the optimization process. As opposed to that, the formulation (7) accommodates the violation without creating any discontinuities.

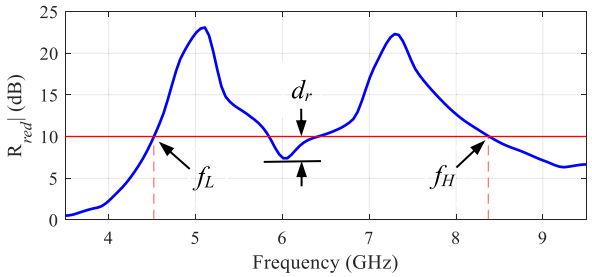

Fig. 6. Exemplary RCS characteristic with the lower frequency f_L, upper frequency f_H, and $r_{\max}$ violation d_r marked to indicate the defining quantities of the objective function for RCS reduction bandwidth improvement.

Let $\boldsymbol{x}_A$ denote the aggregated designable parameter vector of four meta-atoms. Furthermore, let $\boldsymbol{R}_{\mathrm{red}}(\boldsymbol{x}_A, f)$ represent the RCS reduction characteristics over frequency f. The RCS reduction bandwidth B_{RCS} is defined as the continuous range of frequencies satisfying the condition $\boldsymbol{R}_{\mathrm{red}}(\boldsymbol{x}_A, f) \geq r_{\max}$, where $r_{\max}$ stands for acceptance threshold (e.g., 10 or 15 dB).

A practical challenge associated with the standard formulation of the optimization task is that local violations of the condition $\boldsymbol{R}_{\mathrm{red}}(\boldsymbol{x}_A, f) \geq r_{\max}$, unavoidable in the course of the optimization run, lead to discontinuities of the objective function (here, the RCS reduction bandwidth), as shown in Fig. 5. These are problematic to gradient-based optimization algorithms. A workaround is regularization, where violations are incorporated into the objective function without creating discontinuities and large jumps in the (formally defined) bandwidth. A possible formulation is the following, see Fig. 6. Here, f_L and f_H represent the minimum and the maximum frequency for which the condition $\boldsymbol{R}_{\mathrm{red}}(\boldsymbol{x}_A, f) \geq r_{\max}$ is satisfied. Let d_r denote the maximum allowed violation within the frequency interval $[f_L f_H]$. Using these, the objective function U_{RCS} for metasuface optimization will be defined as

$$U_{RCS}(\boldsymbol{x}_A) = -[f_H(\boldsymbol{x}_A) - f_L(\boldsymbol{x}_A)] + \beta c_r(\boldsymbol{x}_A)^2. \quad (7)$$

The first term in (7) is the RCS reduction bandwidth (the minus sign is to convert the problem into a minimization task).

The second component is a regularization term with the function c_r defined as $c_r(\boldsymbol{x}_A) = d_r$ if $d_r > 0$ and zero otherwise. It is introduced to increase the objective function if violation of the acceptance threshold appears. The contribution of the regularization term is controlled by coefficient β. Here, it is set to $\beta = 1$, but this value is not critical. Nevertheless, it can be used to control the tolerance level of d_r.

The formulation (7) efficiently addresses the issues related to the standard formulation, particularly, the in-band violations of the objective function within the potential bandwidth. The parameter adjustment task is formulated as

$$\boldsymbol{x}_A^* = \arg\min_{\boldsymbol{x}_A \in X\times X\times X\times X\times X} U_{RCS}(\boldsymbol{x}_A). \quad (8)$$

Optimization is performed using the TR gradient search algorithm [33], [34]. To expedite the process, the Jacobian matrix of $\boldsymbol{R}_{\text{red}}$ is estimated using finite differentiation in the first iteration and then updated using the rank-one Broyden formula [31] in the subsequent iterations. Typically, the number of EM simulations required to achieve an optimal solution is $M \cdot n$, where n is the number of designable variables, and $M = 3$–4.

IV. Results and Discussion

A. Numerical and Experimental Validation of the Metasurface

This section presents the modeling and optimization results together with the performance evaluation of the optimum meta-atom designs. The design configuration of the coding metasurface is also demonstrated along with its experimental validation, followed by a discussion of its monostatic and bistatic RCS performance.

B. Modeling and Optimization Results of Meta-Atoms

The meta-atom design under consideration [cf. Fig. 1(a)] has three geometry parameters, i.e., p, b, and d. Hence, the vector of designable variables is $\boldsymbol{x} = [p\ b\ d]^T$; L and W are fixed. The parameter space X is determined by the lower and upper bounds $\boldsymbol{l} = [3.5\ 0.3\ 0.2]^T$ and $\boldsymbol{u} = [10\ 1.6\ 2.4]^T$; all dimensions are in mm. The training samples are distributed on a uniform grid $M_{7.12.7}$ (cf. Section III-B) with a total number of $N = 588$ samples. The acquired EM simulation data have been divided into the training (85 percent) and the test data (15 percent), later utilized for model accuracy evaluation. The frequency-domain solver of the CST Microwave Studio is utilized to evaluate the phase reflection responses of the meta-atoms.

The absolute error of the surrogate model is as low as 0.86° (averaged over the testing set) with the standard deviation of 1.7°. These figures demonstrate good predictive power of the surrogate, especially when considering the typical range of the meta-atom phase response (>400°). Fig. 7 shows the surrogate and EM-simulated meta-atom responses at selected test locations. The agreement between the surrogate and EM-simulated responses is excellent.

Having a trained surrogate model, the optimization is performed according to the procedure of Section III-B. The obtained geometries are $\boldsymbol{x}^{(1)*} = [4.222\ 1.6\ 2.175]^T$, $\boldsymbol{x}^{(2)*} = [3.5\ 1.456\ 0.2]^T$, $\boldsymbol{x}^{(3)*} = [3.5\ 1.022\ 0.2]^T$, and $\boldsymbol{x}^{(4)*} = [10\ 0.422\ 0.2]^T$. Fig. 8 shows the designs, classified as "00," "01," "10," and "11." The reflection amplitude and phase responses of the meta-atoms are shown in Fig. 9. The phase difference characteristics are shown in Fig. 10. Note that the condition (1) is approximately satisfied for the frequencies from 20 to about 35 GHz. Consequently, this frequency range can be anticipated as RCS reduction bandwidth of the entire metasurface.

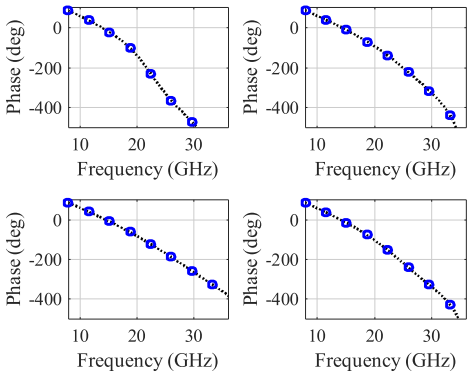

Fig. 7. Performance of the meta-atom surrogate model: EM model (. . .) and surrogate responses (○) at the selected test locations.

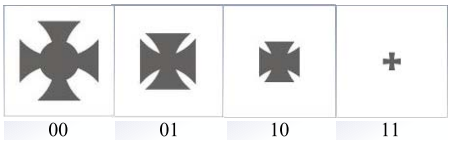

Fig. 8. Specific geometries of the globally optimized meta-atoms.

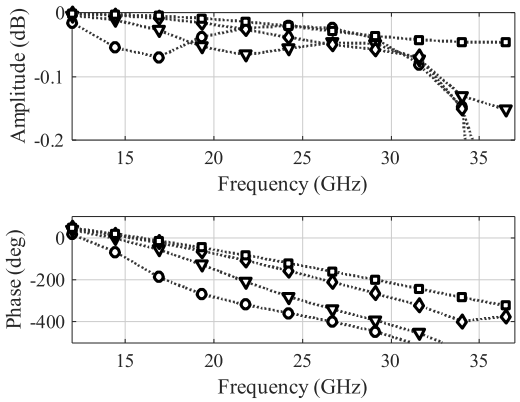

Fig. 9. Reflection performance of the optimized meta-atoms: reflection amplitude (top) and reflection phase (bottom). The responses of "00," "01," "10," and "11" are marked (○), (Δ), (◇), and (□), respectively.

C. Optimization Results of the Entire Metasurface

Upon finding globally optimum meta-atom designs (cf. Section IV-A), the coding metasurface is characterized. For implementing the entire architecture, the periodic lattices consisting of atoms "00," "01," "10," and "11," are arranged in a uniform manner to realize a diffusive coding metasurface.

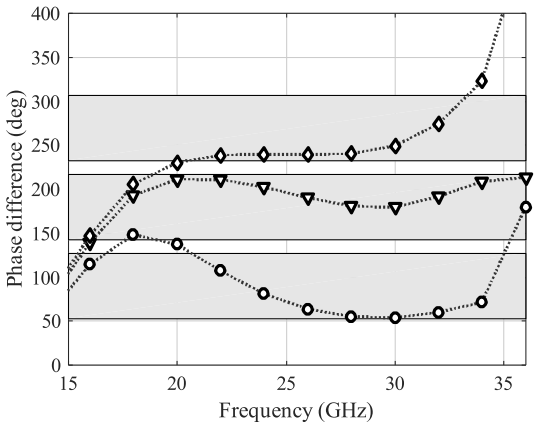

Fig. 10. Reflection phase differences between the optimized meta-atoms. The gray-shaded area indicates the acceptable range according to the condition (1). The differences between atoms "00" and "01," "01" and "10," and "10" and "11" are marked (◯), (Δ), and (◇), respectively.

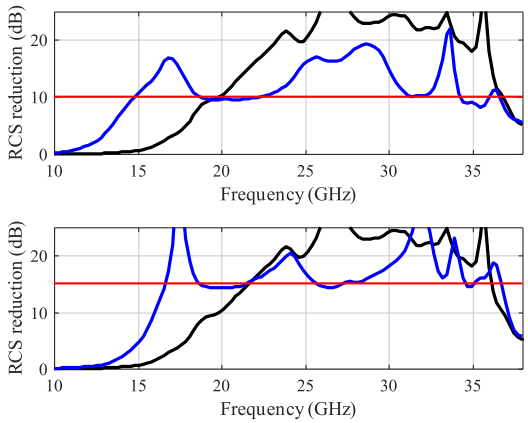

Fig. 12. RCS characteristic of the metasurface optimized for 10-dB (top) and 15-dB (bottom) reduction threshold. The simulated responses after the procedure of Section III-B (black) and after final optimization stage (blue) are shown. The red horizontal line represents the target RCS reduction threshold.

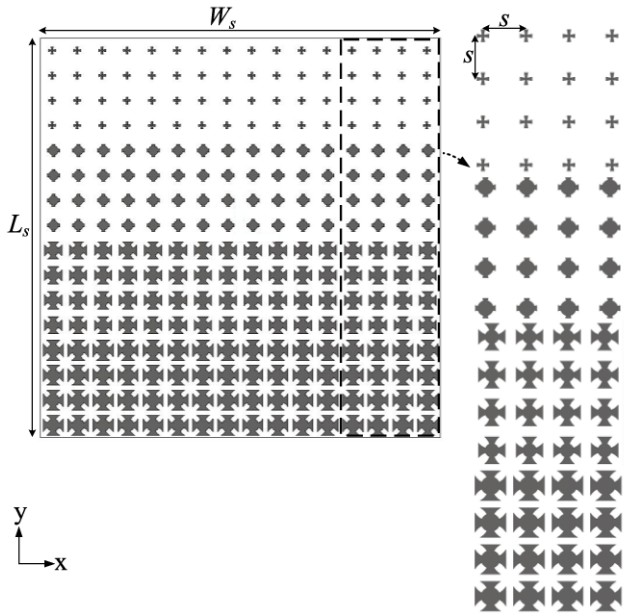

Fig. 11. Configuration of the considered coding metasurface (optimized for 10-dB RCS reduction).

Fig. 11 shows a two-bit coding metasurface comprising sixteen elements: each consisting of four 4×4 periodic lattices of meta-atoms "00," "01," "10," and "11." The overall size of the metasurface is $W_s \times L_s = 96 \times 96$ mm^2. The interelement spacing of individual meta-atoms in the array is $s = 6$ mm. The structure is implemented on a ground-backed Arlon AD250 lossy substrate ($\varepsilon_r = 2.5$, $h = 1.5$ mm, and $\tan\delta = 0.0018$). To test the RCS performance, an equivalent PEC surface is implemented to be utilized as a reference. The time-domain solver of the CST Microwave Studio is utilized for both the monostatic and bistatic RCS analyses.

At this point, the second optimization stage, i.e., EM-driven local refinement of the entire metasurface, is executed (cf. Section III-C). The availability of a good initial design, determined previously, facilitates gradient-based tuning and allows us to identify globally optimum design at acceptable computational expenses. Although finding the global optimum is not formally guaranteed by the procedure, it is very likely due to the global optimality of the meta-atom designs, and the fact is that the phase difference properties (2) are reliable estimators of the RCS reduction bandwidth. Furthermore, to demonstrate the utility of adopted two-stage optimization procedure (i.e., efficacy of the initial and versatility of the final stage), we optimized the metasuface design for two levels of RCS reduction, i.e., 10 and 15 dB. This corroborates that following a systematic design procedure (cf. Section III), the structure can be seamlessly optimized as per the designer's needs.

The designs obtained at the final optimization stages for 10- and 15-dB RCS reduction thresholds are $\boldsymbol{x}_A^* = [3.3978\ 1.6859\ 2.9164\ 3.2022\ 1.4472\ 2.5102\ 5.9794\ 0.8937\ 2.2448\ 8.0707\ 0.7624\ 0.3210]^T$ and $\boldsymbol{x}_B^* = [4.027\ 1.666\ 1.806\ 2.503\ 1.321\ 3.054\ 7.660\ 0.952\ 2.8401\ 9.504\ 0.810\ 0.240]^T$, respectively.

To quantify the improvement obtained in the final optimization stage, the RCS reduction bandwidth achieved upon EM-based tuning is compared to the performance of the structure implemented using the design identified at the initial optimization stage of Section III-B. As mentioned before, the EM-driven optimization is performed for both 10- and 15-dB RCS reduction levels. The results are shown in Fig. 12. It can be observed that the supervised-learning-based design technique already ensures a broadband RCS reduction performance. Moreover, after executing the final optimization stage, the RCS reduction bandwidth noticeably extends, especially toward the lower frequencies. The bandwidth improvement level in the final optimization stage is in the range of 4–5 GHz. For both design scenarios, the RCS reduction occurs in a broad frequency range, i.e., from 14.8 to 37.2 GHz for 10-dB RCS reduction threshold and from 16.7 to 37 GHz for 15-dB threshold.

For better illustration, the far-field scattering performance of a metallic plate, the metasurface optimized for 10 dB, and the metasurface designed for 15-dB RCS reduction level are presented in Fig. 13. The 3-D scattering field distribution is obtained by far-field simulation of the structure. It can be

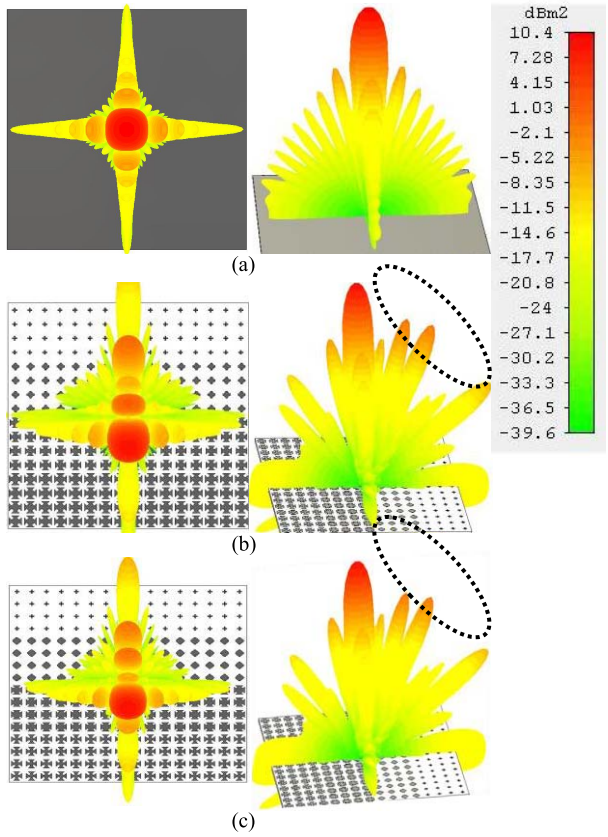

Fig. 13. 3-D scattering performance. (a) PEC surface. Metasurface optimized for (b) 10 dB and (c) 15 dB. The plots correspond to the frequency of 30 GHz.

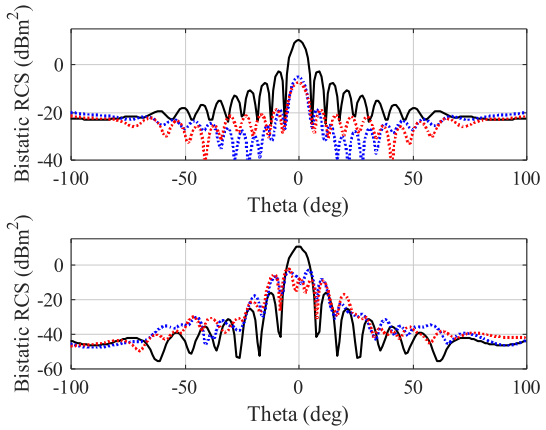

Fig. 14. Bistatic RCS performance at 30 GHz along the principal plane $\phi = 0$ (top) and along the diagonal plane $\phi = 45$ (bottom). The curves corresponding to the design optimized for 10 and 15 dB are marked blue and red, respectively, whereas the black curve indicates the scattered field from the PEC surface.

noticed that the metallic surface causes strong reflections in the boresight direction, in a single lobe, when the plane wave impinges on it. Conversely, the coding metasurface diffuses the incident wave to several directions of the space, which results in a significant reduction of the energy in the vicinity of the scattering peak.

For the sake of supplementary illustration, Fig. 14 shows the bistatic RCS reduction performance of the considered design

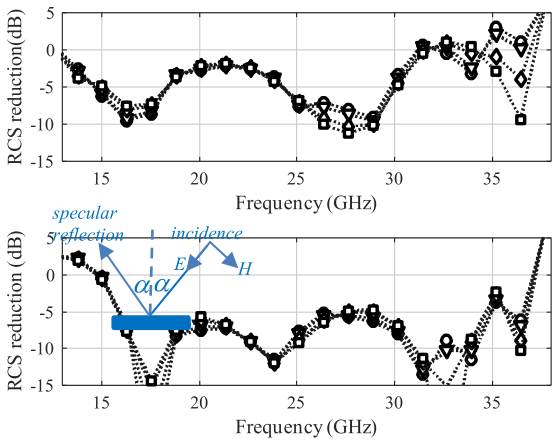

Fig. 15. RCS characteristic in specular directions for 10-dB (top) and 15-dB (bottom) reduction threshold. The responses at $\alpha = 0°$, 30°, 60°, and 90° incident angles are marked (◯), (Δ), (◇), and (□), respectively.

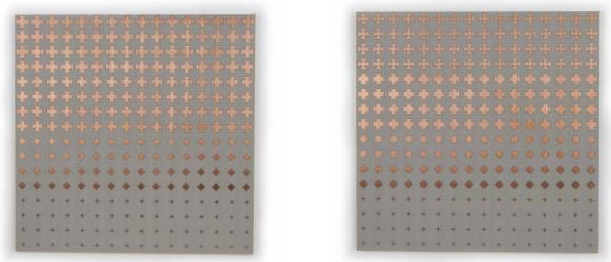

Fig. 16. Photographs of the prototyped metasurfaces: (a) design $\boldsymbol{x}_A^*$ (optimized for 10-dB RCS reduction level) and (b) design $\boldsymbol{x}_B^*$ (optimized for 15-dB RCS reduction level).

at two selected planes. As it can be observed, the reduction very much depends on the selection of the plane, i.e., it is increased whenever the plane misses the scattering lobes and deteriorated otherwise. This only indicates that bistatic performance evaluated at a few selected planes is incapable of giving a full account for the metasurface operation, in contrast to what has been fostered in many related works (see [12]).

To further demonstrate the relevance of the considered design, the sensitivity of its RCS performance to oblique incidence angles has been analyzed. Fig. 15 shows the specular reflection performance of a coding metasurface. The monostatic RCS under the oblique plane wave incidence is the RCS in the specular direction [35]. It can be observed from Fig. 15 that when the incident angle α changes from 0°, 30°, 60°, and 90°, the scattering performance remains almost unaltered. This allows us to conclude that the scattering performance of the metasurface is insensitive to the angle of incidence. In other words, the structure exhibits angularly invariant characteristics.

D. Measurement Setup and Experimental Validation

The two designs presented in Section. IV-B have been fabricated and measured to validate the EM simulation results, cf. Fig. 16. Due to limited amenities, the scattering performance of a coding metasurface has only been evaluated in

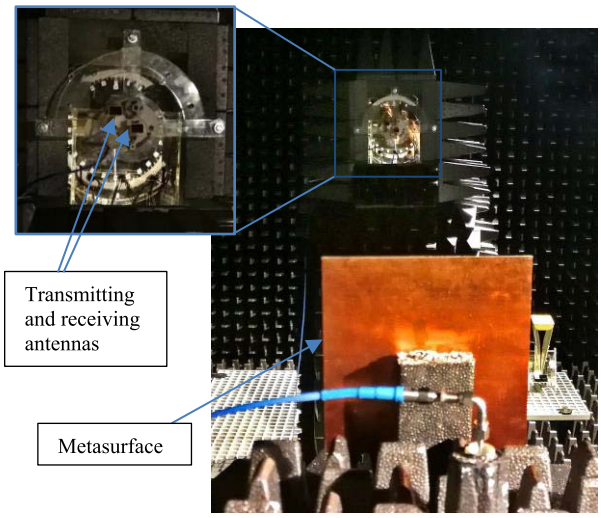

Fig. 17. Measurement setup at Reykjavik University.

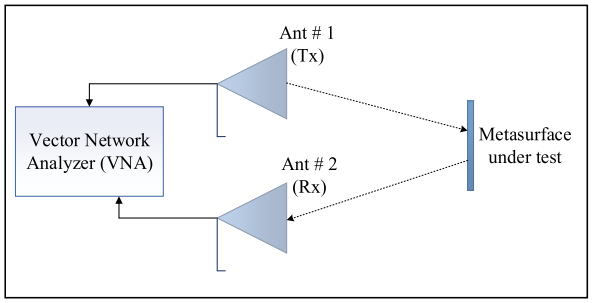

Fig. 18. Block diagram of the measurement environment.

terms of reflectivity using an equivalent metallic surface as a reference to quantify the RCS reduction.

The experimental measurements have been carried out in the anechoic chamber of Reykjavik University and the setup is presented in Fig. 17. The latter consists of a vector network analyzer (VNA) and the two linearly polarized horn antennas (PE9850/2F-15), utilized as the transmitter and the receiver, respectively. The two antennas are positioned perpendicular to the surface under test to realize the normal incidence of the impinging waves and resultant reception of the reflected waves. The distance between the device under test and the antennas is selected to ensure operating in the far-field regime. The schematic of the experimental setup is given in Fig. 18. The scattering performance of the coding metasurface and the corresponding metallic surface is evaluated by measuring the transmission coefficient, captured by the VNA.

The comparison between the measurements and the simulation results is shown in Fig. 19. A decent agreement between the two datasets can be observed. Slight differences can be attributed to several factors. Amidst, the spatial misalignment of the transmitting and receiving antennas with respect to structure under test contributes predominantly. Needless to say, the proper orientation of a surface (realized manually) is a challenging endeavor. A slight misalignment here may lead to considerable discrepancies. However, the measurement data confirm the RCS reduction bandwidth obtained through EM

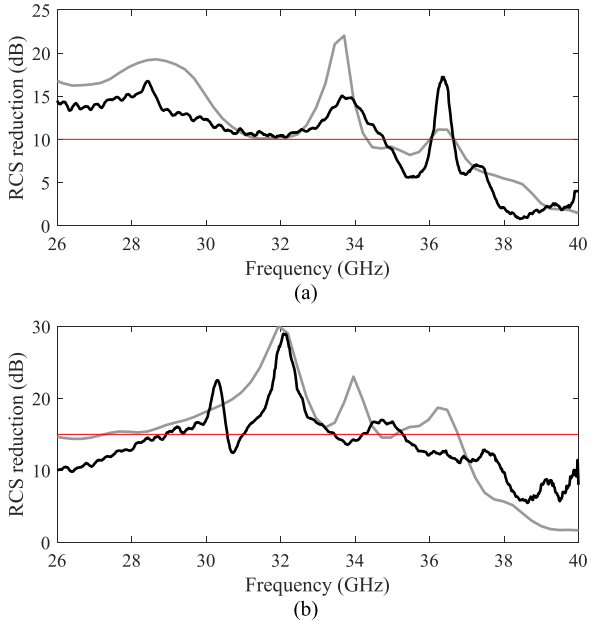

Fig. 19. Measured (black) and simulated (gray) RCS reduction performance comparison for (a) 10- and (b) 15-dB optimized design. The red curve indicates 10- and 15-dB RCS reduction threshold.

TABLE I
CONSIDERED METASURFACE VERSUS STATE-OF-THE-ART DESIGNS

Design	Frequency range (>10-dB RCS reduction) (GHz)	Frequency range (>15-dB RCS reduction) (GHz)	Multiple diffuse scattering (multi-bit)	Angle insensitivity
[20]	7.5–15	8.8–9.1	yes	not studied
[23]	11.95–18.36	12.5–18.2	yes	not studied
[36]	3.75–10	6.5–7.5	no	yes
[37]	8.6–10.7	9.1–10.2	no	yes
[38]	9.7–18.12	11.2–17.1	yes	not studied
[39]	8.8–11	none	yes	not studied
[40]	3.88–4.07	3.95–4.0	no	not studied
[41]	7.98–16.32	9.7–14.5	no	yes
[42]	6.94–9.23	7.2–9.1	yes	yes
[15]	17–42	22–28	no	yes
[16]	5.4–7.4	5.6–6.8	no	yes
This work	14.8–37.2	16.7–37	yes	yes

simulation for both 10- and 15-dB thresholds in the frequency range of 26.5 and 40 GHz. The measurement frequency range is limited by the available hardware. The above findings allow us to conclude that the coding metasurface developed using our algorithmic framework features low observable property in a broad frequency range, and therefore, it has the potential to replace the metallic surfaces in applications where high stealthiness is essential.

E. Benchmarking

The coding metasurface discussed in this work has been benchmarked against the state-of-the-art structures from the

literature. The comparison is carried out in terms of RCS reduction bandwidth, the level of reduction, and the scattering performance in specular directions. The results are given in Table I. As indicated, the design developed using the proposed algorithmic tools clearly outperforms other structures (based upon multiple diffusive scattering) in terms of RCS reduction bandwidth and level of RCS reduction. Furthermore, our design is competitive to similar structures (based upon single-bit coding scheme) in terms of all of the considered performance figures. In addition, our design covers two major radar frequency bands K and Ka, as well as a part of the Ku-band. Therefore, it has the potential to surpass other structures proposed for stealth applications.

V. Conclusion

This article presents the algorithmic approach developed for global optimization of multibit coding metasurfaces. The adopted optimization framework offers new ways of controlling the peak RCS reduction threshold, as well as enable broadband RCS reduction. The metasurface is characterized by a two-bit coding scheme, i.e., it consists of four unique meta-atom geometries denoted as "00," "01," "10," and "11" binary codes, each representing the phase reflection states of 0, $\pi/2$, π, and $3\pi/2$, respectively.

A rigorous design approach, combining global surrogate-assisted optimization of meta-atoms and EM-driven tuning of the entire metasurface, turns out to be critical to achieve the aforementioned level of performance. A supervised-learning-based technique is initially employed to determine globally optimum meta-atom designs, subsequently used as the building blocks of the coding metasurface. The former involves a fast surrogate model that facilitates exploration of the parameter space, otherwise prohibitive due to a massive number of expensive EM-simulations involved. Still, a concurrent optimization of four meta-atoms entails combinatorial explosion, which hinders the utilization of the standard global exploration techniques. A sequential-search strategy has been developed specifically to address this issue. The final stage involves direct EM-driven optimization of the entire structure, oriented toward maximization of the RCS reduction bandwidth. The structure has been optimized for two levels of RCS reduction, i.e., 10 and 15 dB. The performance of the metasurface design considered as an illustration example is investigated using monostatic and bistatic scattering properties, indicating that the RCS reduction is realized in a broad frequency range, i.e., from 14.8 to 37.2 GHz for 10-dB RCS reduction level and from 16.7 to 37 GHz for 15-dB level. The prototypes have been fabricated to corroborate the simulation results. A good agreement between the two datasets has been observed. Both structures have been benchmarked against state-of-the-art designs and demonstrated to be superior in terms of the RCS reduction bandwidth and the level of RCS reduction.

Acknowledgment

The authors would like to thank Dassault Systemes, France, for making CST Microwave Studio available.

References

[1] G. A. Rao and S. P. Mahulikar, "Integrated review of stealth technology and its role in airpower," *Aeronaut. J.*, vol. 106, no. 1066, pp. 629–642, Dec. 2002.

[2] E. F. Knott, *Radar Cross Section Measurements*. Cham, Switzerland: Springer, 2012, pp. 12–36.

[3] P. Westwick, *Stealth: The Secret Contest to Invent Invisible Aircraft*. London, U.K.: Oxford Univ. Press, 2019, pp. 5–42.

[4] T. A. Khan, J. X. Li, Z. Li, M. Abdullah, J. Chen, and A. X. Zhang, "Design of Vivaldi antenna with wideband reduced radar cross section," *AEU Int. J. Electron. Commun.*, vol. 95, pp. 47–51, Oct. 2018.

[5] T. J. Cui, D. R. Smith, and R. Liu, *Metamaterials Theory, Design, and Applications*. New York, NY, USA: Springer, 2010.

[6] N. I. Landy, S. Sajuyigbe, J. J. Mock, D. R. Smith, and W. J. Padilla, "Perfect metamaterial absorber," *Phys. Rev. Lett.*, vol. 100, no. 20, pp. 207–402, 2008.

[7] F. Costa, A. Monorchio, and G. Manara, "Analysis and design of ultra thin electromagnetic absorbers comprising resistively loaded high impedance surfaces," *IEEE Trans. Antennas Propag.*, vol. 58, no. 5, pp. 1551–1558, May 2010.

[8] Y. Liu and X. Zhao, "Perfect absorber metamaterial for designing low-RCS patch antenna," *IEEE Antennas Wireless Propag. Lett.*, vol. 13, pp. 1473–1476, 2014.

[9] N. Yu *et al.*, "Light propagation with phase discontinuities: Generalized laws of reflection and refraction," *Science*, vol. 334, no. 6054, pp. 333–337, Oct. 2011.

[10] X. Gao, X. Han, W.-P. Cao, H. O. Li, H. F. Ma, and T. J. Cui, "Ultrawideband and high-efficiency linear polarization converter based on double V-shaped metasurface," *IEEE Trans. Antennas Propag.*, vol. 63, no. 8, pp. 3522–3530, Aug. 2015.

[11] M. Paquay, J.-C. Iriarte, I. Ederra, R. Gonzalo, and P. de Maagt, "Thin AMC structure for radar cross-section reduction," *IEEE Trans. Antennas Propag.*, vol. 55, no. 12, pp. 3630–3638, Dec. 2007.

[12] J. C. Iriarte Galarregui, A. Tellechea Pereda, J. L. M. de Falcon, I. Ederra, R. Gonzalo, and P. de Maagt, "Broadband radar cross-section reduction using AMC technology," *IEEE Trans. Antennas Propag.*, vol. 61, no. 12, pp. 6136–6143, Dec. 2013.

[13] W. Chen, C. A. Balanis, and C. R. Birtcher, "Checkerboard EBG surfaces for wideband radar cross section reduction," *IEEE Trans. Antennas Propag.*, vol. 63, no. 6, pp. 2636–2645, Jun. 2015.

[14] K. Wang, J. Zhao, Q. Cheng, D. S. Dong, and T. J. Cui, "Broadband and broad-angle low-scattering metasurface based on hybrid optimization algorithm," *Sci. Rep.*, vol. 4, no. 1, May 2015, Art. no. 5935.

[15] H. Sun *et al.*, "Broadband and broad-angle polarization-independent metasurface for radar cross section reduction," *Sci. Rep.*, vol. 7, no. 1, Jan. 2017, Art. no. 40778.

[16] X. Liu, J. Gao, L. Xu, X. Cao, Y. Zhao, and S. Li, "A coding diffuse metasurface for RCS reduction," *IEEE Antennas Wireless Propag. Lett.*, vol. 16, pp. 724–727, May 2017.

[17] S. Sui *et al.*, "Absorptive coding metasurface for further radar cross section reduction," *J. Phys. D, Appl. Phys.*, vol. 51, no. 6, Feb. 2018, Art. no. 065603.

[18] Y. Zhao *et al.*, "Broadband diffusion metasurface based on a single anisotropic element and optimized by the simulated annealing algorithm," *Sci. Rep.*, vol. 6, no. 1, Jul. 2016, Art. no. 23896.

[19] L. Ali, Q. Li, T. A. Khan, J. Yi, and X. Chen, "Wideband RCS reduction using coding diffusion metasurface," *Materials*, vol. 12, no. 17, p. 2708, Aug. 2019.

[20] T. J. Cui, M. Q. Qi, X. Wan, J. Zhao, and Q. Cheng, "Coding metamaterials, digital metamaterials and programmable metamaterials," *Light, Sci. Appl.*, vol. 3, no. 10, Oct. 2014, Art. no. 218.

[21] L. Liang *et al.*, "Broadband and wide-angle RCS reduction using a 2-bit coding ultrathin metasurface at terahertz frequencies," *Sci. Rep.*, vol. 6, no. 1, Dec. 2016, Art. no. 39252.

[22] C. Huang, B. Sun, W. Pan, J. Cui, X. Wu, and X. Luo, "Dynamical beam manipulation based on 2-bit digitally-controlled coding metasurface," *Sci. Rep.*, vol. 7, no. 1, Sep. 2017, Art. no. 42302.

[23] M. Feng *et al.*, "Two-dimensional coding phase gradient metasurface for RCS reduction," *J. Phys. D, Appl. Phys.*, vol. 51, Aug. 2018, Art. no. 375103.

[24] S. Koziel and A. Pietrenko-Dabrowska, "Efficient gradient-based algorithm with numerical derivatives for expedited optimization of multi-parameter miniaturized impedance matching transformers," *Radioengineering*, vol. 27, no. 3, pp. 572–578, Sep. 2019.

[25] T. W. Simpson, J. D. Poplinski, P. N. Koch, and J. K. Allen, "Metamodels for computer-based engineering design: Survey and recommendations," *Eng. Comput.*, vol. 17, no. 2, pp. 129–150, Jul. 2001.
[26] S. Koziel, L. Leifsson, and X. S. Yang, "Surrogate-based optimization," in *Simulation-Driven Design Optimization and Modeling for Microwave Engineering*, S. Koziel, X. S. Yang, and Q. J. Zhang, Eds. London, U.K.: Imperial College Press, 2012, pp. 41–80.
[27] S. Koziel and J. W. Bandler, "Reliable microwave modeling by means of variable-fidelity response features," *IEEE Trans. Microw. Theory Techn.*, vol. 63, no. 12, pp. 4247–4254, Dec. 2015.
[28] S. Koziel and A. Pietrenko-Dabrowska, *Performance-Driven Surrogate Modeling of High-Frequency Structures*. New York, NY, USA: Springer, 2020.
[29] F. Feng *et al.*, "Multifeature-assisted neuro-transfer function surrogate-based EM optimization exploiting trust-region algorithms for microwave filter design," *IEEE Trans. Microw. Theory Techn.*, vol. 68, no. 2, pp. 531–542, Feb. 2020.
[30] X. Chen, W. Xue, H. Shi, J. Yi, and W. E. I. Sha, "Orbital angular momentum multiplexing in highly reverberant environments," *IEEE Microw. Wireless Compon. Lett.*, vol. 30, no. 1, pp. 112–115, Jan. 2020.
[31] S. Koziel and A. Pietrenko-Dabrowska, "Expedited optimization of antenna input characteristics with adaptive Broyden updates," *Eng. Comput.*, vol. 37, no. 3, pp. 851–862, Sep. 2019.
[32] S. Koziel and M. Abdullah, "Machine-learning-powered EM-based framework for efficient and reliable design of low scattering metasurfaces," *IEEE Trans. Microw. Theory Techn.*, vol. 69, no. 4, pp. 2028–2041, Apr. 2021.
[33] A. R. Conn, N. I. M. Gould, and P. L. Toint, *Trust Region Methods* (MPS-SIAM Series on Optimization). Philadelphia, PA, USA: Society for Industrial and Applied Mathematics, 2000.
[34] S. Koziel, J. W. Bandler, and Q. S. Cheng, "Robust trust-region space-mapping algorithms for microwave design optimization," *IEEE Trans. Microw. Theory Techn.*, vol. 58, no. 8, pp. 2166–2174, Aug. 2010.
[35] Y. Zhuang *et al.*, "Random combinatorial gradient metasurface for broadband, wide-angle and polarization-independent diffusion scattering," *Sci. Rep.*, vol. 7, no. 1, pp. 1–10, Dec. 2017.
[36] A. Y. Modi, C. A. Balanis, C. R. Birtcher, and H. N. Shaman, "Novel design of ultrabroadband radar cross section reduction surfaces using artificial magnetic conductors," *IEEE Trans. Antennas Propag.*, vol. 65, no. 10, pp. 5406–5417, Oct. 2017.
[37] Y. Zhuang, G. Wang, J. Liang, T. Cai, W. Guo, and Q. Zhang, "Flexible and polarization-controllable diffusion metasurface with optical transparency," *J. Phys. D, Appl. Phys.*, vol. 50, no. 46, Nov. 2017, Art. no. 465102.
[38] Q. Zheng *et al.*, "Wideband, wide-angle coding phase gradient metasurfaces based on pancharatnam-berry phase," *Sci. Rep.*, vol. 7, no. 1, Apr. 2017, Art. no. 43543.
[39] Y. Zhuang, G. Wang, T. Cai, and Q. Zhang, "Design of bifunctional metasurface based on independent control of transmission and reflection," *Opt. Exp.*, vol. 26, no. 3, pp. 3594–3603, Feb. 2018.
[40] L. Shao, M. Premaratne, and W. Zhu, "Dual-functional coding metasurfaces made of anisotropic all-dielectric resonators," *IEEE Access*, vol. 7, pp. 45716–45722, 2019.
[41] S. H. Kim and Y. J. Yoon, "Wideband radar cross-section reduction on checkerboard metasurfaces with surface wave suppression," *IEEE Antennas Wireless Propag. Lett.*, vol. 18, no. 5, pp. 896–900, May 2019.
[42] X. Han *et al.*, "Multiple diffuse coding metasurface of independent polarization for RCS reduction," *IEEE Access*, vol. 8, pp. 162313–162321, 2020.

Muhammad Abdullah received the B.Sc. degree from the University of Engineering and Technology, Lahore, Pakistan, in 2016, and the M.Sc. degree from Xi'an Jiaotong University (XJTU), Xi'an, China, in 2019.

Since late 2019, he has been with the Department of Engineering, Reykjavik University, Reykjavik, Iceland, as a Researcher. From 2018 to 2019, he was with the Electromagnetics and Communication Laboratory, XJTU. His broader research interests include surrogate-based modeling and optimization, CAD and modeling of antennas and other high-frequency structures, MIMO antennas, simulation-driven design, and machine-learning techniques.

Mr. Abdullah received the excellent master's thesis award on completion of the M.Sc. degree.

Slawomir Koziel (Senior Member, IEEE) received the M.Sc. and Ph.D. degrees in electronic engineering from the Gdansk University of Technology, Gdansk, Poland, in 1995 and 2000, respectively, and the M.Sc. degrees in theoretical physics and mathematics and the Ph.D. degree in mathematics from the University of Gdansk, Gdansk, in 2000, 2002, and 2003, respectively.

He is currently a Professor with the Department of Engineering, Reykjavik University, Reykjavik, Iceland. His research interests include CAD and modeling of microwave and antenna structures, simulation-driven design, surrogate-based optimization, space mapping, circuit theory, analog signal processing, evolutionary computation, and numerical analysis.